Calculation of gas heating in direct current argon glow discharges

Annemie Bogaerts[a] and Renaat Gijbels
Department of Chemistry, University of Antwerp, Universiteitsplein 1, B-2610 Wilrijk-Antwerp, Belgium

Vladimir V. Serikov
Simulation Group, Production Engineering Center, Nippon Sheet Glass Company Ltd., Anesaki-kaigan 6, Ichihara-city, Chiba, 299-0107 Japan

(Received 24 September 1999; accepted for publication 13 March 2000)

A model is developed for self-consistently calculating the gas temperature in a direct current argon glow discharge, used for analytical spectroscopy. The power input into the argon gas due to elastic (i.e., kinetic energy transfer) collisions of Ar^+ ions, and fast Ar atoms, sputtered Cu atoms and electrons with the argon gas atoms is calculated with Monte Carlo models. This power input is used in a heat transfer model to calculate the gas temperature. The amount of power input, the contributions of the various input sources, and the resulting gas temperature are calculated for a wide range of voltages, pressures, and currents, typically applied in analytical spectroscopy. It is found that the temperature can increase significantly at high voltages, pressures, and currents (up to a factor of 3 compared to absolute room temperature). © *2000 American Institute of Physics.* [S0021-8979(00)04012-3]

I. INTRODUCTION

Glow discharges are employed in a large number of fields, e.g., in the semiconductor industry for etching and deposition purposes, as lasers, light sources, and in displays. Moreover, they are also being applied in analytical chemistry as spectroscopic sources for the analysis of mainly solid samples by mass spectrometry or optical emission spectrometry.[1,2] In the latter case, the cathode is constructed from the material to be analyzed, which is sputter bombarded by plasma particles, resulting in a sputtered atom population in the plasma representative of the cathode sample. These atoms can be ionized, and the ions can be measured in a mass spectrometer, giving rise to glow discharge mass spectrometry (GDMS). Moreover, the atoms can also be excited in the plasma, followed by radiative decay, and the resulting photons, characteristic of the material to be analyzed, can be detected in an optical emission spectrometer, leading to glow discharge optical emission spectrometry (GD–OES).

In order to improve the results in these applications, clear insight in the glow discharge processes is desirable. This can be obtained by numerical modeling. In recent years, we have developed a model network for dc glow discharges used in analytical chemistry, consisting of several submodels (Monte Carlo, fluid, and collisional-radiative models) for the various plasma species [electrons, argon ions (Ar^+, Ar^{2+}, and Ar_2^+), fast argon atoms, argon atoms in various excited levels, sputtered atoms, and ions, both in the ground state and in various excited levels] (e.g., Refs. 3–14). Reasonable agreement with experimental data has been reached in the calculated current–voltage characteristics, the densities of various plasma species (electrons, argon metastable atoms, sputtered atoms, and ions), the crater profiles and erosion rates due to cathode sputtering, the optical emission intensities of spectral lines, etc. (e.g., Ref. 13). However, it was also found that some input parameters, like the pressure and gas temperature, have significant effects on the calculated quantities like the electrical current. Indeed, a variation of 30% in the gas pressure or temperature resulted in a change by about a factor of 2 in the calculated current, due to a positive feedback effect (i.e., a higher gas pressure or lower gas temperature yielded a higher gas density, and hence, more ionization collisions and the production of more electrons, which in turn give rise to more ionization collisions, etc., so that the electron and ion fluxes, and from these also the electrical current, increase more than linearly).

Since these two input parameters in the model have such an effect on the calculation results, it would be desirable to know them with high accuracy. However, such accuracy is, in practice, difficult to achieve. Especially in commercial instruments for analytical GDMS and GD–OES, the gas pressure can generally not be measured. Moreover, the actual value of the gas temperature is even more uncertain. Mostly it is assumed, for typical GDMS conditions (pressure around 50–100 Pa, voltage between 500 and 1500 V, and current between 1 and 10 mA), that the gas temperature is only slightly above room temperature. On the other hand, gas temperatures were measured in a standard Grimm-type source that has been used for GD–OES (pressure of several hundred pascal, voltage of 500–1500 V and current between 10 and 100 mA), and typical values of 600–1400 K were obtained, increasing with current.[15] It is indeed to be expected that the gas temperature will increase with discharge power, but the exact values are generally not known.

In order to make an estimate of the gas temperature in a glow discharge at typical analytical operating conditions (both for GDMS and GD–OES), and to obtain a better insight in the phenomenon of gas heating in glow discharges in general, we have developed a model to describe the energy

[a]Author to whom correspondence should be addressed; electronic mail: bogaerts@uia.ua.ac.be

transfer into the argon gas due to various collision processes, and to calculate the resulting temperature increase. This phenomenon of gas heating in glow discharges and related plasmas has been studied in several papers (e.g., Refs. 15–26), either by experiments (by measuring the Doppler broadening,[15] by sampling the relative pressure with a probe[16] or by measuring the Rayleigh scattering),[17,18] simple empirical models,[16] fluid models (based on a gas energy balance equation)[19,20] or more explicit models based on Monte Carlo methods.[21–26] However, these papers usually describe magnetron discharges or inductively coupled plasmas, which operate at much lower pressures (millitorr range),[16–19,21–24,26] or on the contrary, at much higher pressures (100 Torr range).[20] Only Refs. 15 and 25 describe discharge conditions similar to those in which we are interested. In the present article, we follow a similar approach to the one in Ref. 24. The glow discharge is described self-consistently by a series of models (Monte Carlo, fluid, and collisional-radiative models; see earlier and Refs. 3–14). The energy transfer to the argon gas atoms, due to various processes (i.e., collisions, reflection at the walls, thermalization) of argon ions, fast argon atoms, sputtered atoms, and electrons, is calculated by Monte Carlo models. The resulting temperature increase is then calculated with the heat conduction equation. This model is explained in more detail in Sec. II. Section III presents the results for a range of analytical GDMS and GD–OES discharge conditions (see earlier), as well as a discussion about the effect of input parameters such as thermal accommodation coefficient, cathode temperature, and energy threshold for the beam and bulk argon atoms (see later). Finally, a conclusion will be given in Sec. IV.

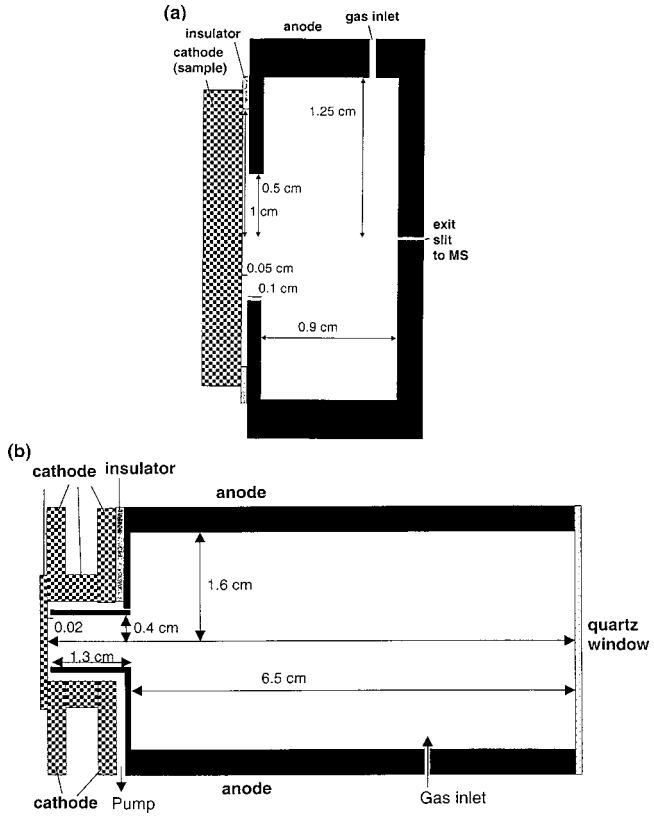

FIG. 1. Schematic pictures of the VG9000 cell (a) and the Grimm-type cell (b), typically used for GDMS and GD–OES.

II. DESCRIPTION OF THE MODEL

A. General

The model is developed for typical cell geometries used for commercial applications of GDMS and GD–OES, i.e., the VG9000 cell for flat samples (VG Elemental, Thermo; for GDMS) and the Grimm-type source (used in all commercial GD–OES instruments). Schematic pictures of these cell geometries are shown in Figs. 1(a) and 1(b), respectively. The conditions investigated for the VG9000 cell are 50–100 Pa, 600–1400 V, and 1–10 mA, which are typical for GDMS, whereas the conditions under study for the Grimm-type cell are 200–500 Pa, 500–1200 V, and 10–100 mA, which are commonly used for GD–OES.

The species assumed to be present in the plasma, and described in the model, are the argon gas atoms (Ar^0), argon ions (Ar^+, Ar^{2+}, and Ar_2^+), fast argon atoms created from the Ar^+ ions and Cu^0 atoms by collisions (Ar_f^0), argon atoms in various excited levels (Ar*), electrons, sputtered atoms (copper is taken as an example, Cu^0), copper ions (Cu^+), and copper atoms and ions in excited levels (Cu* and Cu^{+*}). More information about the description of these species can be found in Refs. 3–14. In the present article, we will focus on the contributions of these species to gas heating.

The sources of argon gas heating (i.e., kinetic energy deposition in the argon gas), taken into account in the model, are the following:

(1) elastic collisions of the Ar^+ ions with Ar^0 atoms (both with isotropic scattering and with backscattering, as an approximation to charge transfer),[27]
(2) elastic collisions of the sputtered Cu^0 atoms with Ar^0 atoms,
(3) elastic collisions of Ar_f^0 atoms with Ar^0 atoms,
(4) elastic collisions of electrons with Ar^0 atoms, and
(5) reflection of Ar^+ ions and Ar_f^0 atoms at the cell walls (the ions are hereby assumed to be 100% neutralized).

Other processes (energy transfer to argon atoms due to other plasma species) are neglected, due to the lower density of these other species. In fact, energy transfer due to elastic collisions of electrons with Ar^0 atoms is also expected to be negligible due to the large mass difference. However, since gas heating models have never been developed for analytical glow discharges before, we wanted to incorporate this collision mechanism in our model, to obtain a better feeling about its relative contribution.

As mentioned before, the energy transfer by the earlier-mentioned sources is described in Monte Carlo models, and the resulting temperature rise is calculated with the heat conduction equation. In the following, these models are explained in some more detail.

B. Monte Carlo models

We have previously developed some Monte Carlo models for the Ar^+ ions, the Ar_f^0 atoms, the Cu^0 atoms and the electrons,[3,4,7] and the complete explanation of these models will not be repeated here. Only a brief description will be given.

The Ar^+ **ions** are followed in the cathode dark space (CDS) in front of the cathode, where a strong electric field is present. The latter is calculated self-consistently from a fluid model for electrons and argon ions. The Ar^+ ions are not followed in the negative glow (NG), because the electric field is very weak there, and the ions are assumed to be thermalized. Hence, they will not give energy to the argon background gas. The Ar^+ ions enter the CDS from the NG (determined from the ion flux, calculated in the fluid model). A large number of ions are followed, one after the other, during successive time steps. Their trajectory is calculated with Newton's laws, and the collisions are treated with random numbers (i.e., occurrence of a collision, kind of the collision and new energy and direction after the collision). Collision processes incorporated in this Ar^+ Monte Carlo model comprise elastic collisions with Ar^0 gas atoms [both with isotropic scattering and with backscattering (i.e., so-called charge transfer)],[27] and fast argon ion impact ionization and excitation of the Ar gas. Only collisions with Ar gas atoms are considered, because other species have much lower densities in the plasma. Besides the ions entering from the NG, also ions formed in the CDS by electron, fast argon ion, and atom impact ionization are followed. All the ions are followed during these successive time steps until they collide at the cell walls, where it is assumed that they are all neutralized, being either thermally accommodated or reflected as neutrals with a certain energy. In practice, most ions will bombard the cathode, directed by the strong electric field in front of it.

The Ar_f^0 **atoms**, formed by collisions of Ar^+ ions, Ar_f^0 atoms, Cu^0 atoms or electrons with the Ar^0 gas atoms, are not only followed in the CDS but also in the NG. Indeed, although most of them are created in the CDS, they are not directed to the cathode by the electric field, like the ions, but they can also move to the NG where they collide with Ar gas atoms and give rise to some gas heating. The principle of this Monte Carlo model is the same as for the Ar^+ ions. Collision processes considered in this model are elastic collisions with the Ar^0 gas atoms, and fast argon atom impact ionization and excitation of the Ar gas. Again, only collisions with Ar^0 gas atoms are taken into account. These Ar_f^0 atoms are followed until they collide at the walls, where there is a chance that they become thermally accommodated (defined by the thermal accommodation coefficient α; see later) or reflected, or until they become thermalized in the plasma due to collisions. More information about the Monte Carlo models of Ar^+ ions and Ar_f^0 atoms can be found in Refs. 3 and 7.

The **sputtered** Cu^0 **atoms** are followed with a Monte Carlo model in the entire discharge, until they are thermalized. Indeed, when they are sputtered from the cathode, they have energies in the order of 5–10 eV, and they lose these energies almost immediately due to elastic collisions with the Ar^0 gas atoms. This is the only collision process incorporated in the model, since other collisions with Ar atoms have much lower cross sections, and collisions with other plasma species are unimportant due to their lower densities. This Monte Carlo model is run in the same way as the Ar^+ and Ar_f^0 Monte Carlo models, until the Cu^0 atoms become thermalized in the plasma or at the cell walls, similarly to the Ar_f^0 atoms. We have assumed a sticking coefficient of 0.5 for the Cu atoms at both cathode and anode walls. In practice, we found that the value of the sticking coefficient had no effect on the present calculations, because almost all Cu atoms become thermalized within a few millimeters of the cathode, at the typical pressures under consideration ($\sim$ order of 100 Pa).[4] More details about this model are given in Ref. 4.

Finally, the **electrons** are also followed with a Monte Carlo model in the entire discharge. Collision processes incorporated in the model include electron impact excitation and ionization from the argon ground state and from various argon excited levels, momentum transfer collisions with argon gas atoms, and electron–electron Coulomb collisions. The electrons are followed until they collide at the walls (where they can be absorbed, reflected, or cause secondary electron emission) or until they are slowed down till energies below 0.001 eV.

From these Monte Carlo models, the energy transfer from the Ar^+ ions, Ar_f^0 atoms, Cu^0 atoms, and electrons to the Ar^0 gas atoms is calculated. First, a threshold energy ($E_{\text{threshold}}$) needs to be defined to distinguish the Ar^0 gas atoms (i.e., bulk equilibrium gas) from the fast Ar_f^0 atoms (i.e., beam of particles). Indeed, the concept of temperature is typical for a gas in thermodynamic equilibrium. Therefore, the gas temperature to be defined is characteristic for the bulk equilibrium gas. In Ref. 24 it was found that a threshold energy equal to $9\times$thermal energy ($9\times 3/2kT_{\text{Ar}}$) yielded good results. Hence, we will adopt this value here, although later in this article, we will investigate the effect of this parameter in more detail.

This threshold energy determines whether the energy transferred to the Ar^0 gas atoms in a collision results in the formation of a fast Ar_f^0 atom or only in a temperature rise of the Ar gas (i.e., when the energy of the Ar^0 atoms after the collision is higher or lower than $9E_{\text{thermal}}$, respectively). The energy transfer to the Ar^0 gas atoms is then calculated as follows:

(1) In a collision of Ar^+ ions, Ar_f^0 atoms, Cu^0 atoms or electrons with Ar gas atoms: if $E_{\text{Ar,after coll}} < E_{\text{threshold}}$: we add "$E_{\text{Ar,after coll}} - E_{\text{Ar,before coll}}$" to the energy transfer term. (The energy before the collision is taken from the Maxwell distribution at the argon gas temperature).

(2) Similarly, if in such a collision: $E_{\text{Ar,after coll}} > E_{\text{threshold}}$, an Ar^0 atom becomes fast, and disappears from the bulk Ar gas group. Hence, we subtract "$E_{\text{Ar,before coll}}$" from the energy transfer term.

(3) When the energy of the Ar_f^0 atoms drops below $E_{\text{threshold}}$ due to a collision, the Ar^0 atoms join again the bulk Ar^0 group, and we add their post-collision energy, "$E_{\text{Ar,after coll}}$", to the energy transfer term.

(4) When the Ar^+ ions or Ar_f^0 atoms collide at the walls, a fraction of them, defined by α (see later) will become thermally accommodated, and disappears from the Monte Carlo model. The remaining fraction $(1-\alpha)$ will be reflected as Ar atoms, with an energy given by: $E_{\mathrm{Ar,reflected}}=E_{\mathrm{Ar,in}}-YE_{\mathrm{sp}}$, where $E_{\mathrm{Ar,in}}$ is the energy of the incoming Ar^+ ion or Ar_f^0 atom, Y is the sputtering yield at this incoming energy, and E_{sp} is the energy of the sputtered atoms (both calculated like in Ref. 4). If $E_{\mathrm{Ar,reflected}}>E_{\mathrm{threshold}}$, a fast Ar_f^0 is created which is again followed in the Monte Carlo model, and there is no energy transfer to the Ar gas. If, however, $E_{\mathrm{Ar,reflected}}<E_{\mathrm{threshold}}$, this value of ''$E_{\mathrm{Ar,reflected}}$'' is added to the energy transfer term.

The energy transfer term is in this way calculated in each cell (z,r) of the two-dimensional grid. To obtain the energy transfer per cubic centimeter, it must be divided by the cell volume $(dz2\pi rdr)$. Finally, the calculation was performed for a fixed number of particles in the Monte Carlo models; this number corresponds to a real flux of particles, in s^{-1}. This yields finally the energy transfer term in watts per cubic centimeter, which is used as power input in the heat transfer model.

C. Heat transfer model

This model consists of the solution of the heat conduction equation[24]

$$\frac{\partial^2 T_g}{\partial z^2}+\frac{1}{r}\frac{\partial}{\partial r}\left(r\frac{\partial T_g}{\partial r}\right)=-\frac{P}{\kappa}, \tag{1}$$

where T_g is the argon gas temperature, as a function of z and r position, P is the power input from the Monte Carlo models, and κ is the thermal conductivity $(=1.8\times10^{-4}\,\mathrm{W\,cm^{-1}\,K^{-1}}$ for argon).

The boundary condition of this equation is given by[24,28]

$$T_{g(\mathrm{wall})}=T_{\mathrm{wall}}+\lambda(\nabla T_g)_{\mathrm{wall}}, \tag{2}$$

where

$$\lambda=\frac{2-\alpha}{\alpha}\xi\xi_0\frac{T(\mathrm{K})}{p(\mathrm{Pa})\sigma_T(m^2)} \quad \text{and} \quad \xi=\frac{C_p+\frac{5}{4}R}{C_p-\frac{1}{2}R}. \tag{3}$$

Further, $\xi_0=0.6505\times10^{-23}$, T and p are the temperature and pressure (in kelvin and pascal, respectively), σ_T is the total cross section for argon–argon collisions (taken here as $42\times10^{-20}\,\mathrm{m^2}$), C_p is the specific heat per mole at constant pressure, and α is the thermal accommodation coefficient. This value can vary in the limit between 0 (100% pure elastic reflection) and 1 (100% thermal accommodation: the reflected particles have an energy equal to the wall temperature). There is not a lot of information available in the literature about thermal accommodation coefficients. Winters and co-workers[29] measured the accommodation coefficients for Ar^+ ions (5–4000 eV) on gold and Pt(111) surfaces, and they obtained values in the order of 0.6 for 10 eV, 0.75 for 100 eV, and >0.8 for 200 eV and higher. Below 10 eV, the accommodation coefficients appeared to drop to low values (extrapolated to ~0.2 at 0 eV).[29] Moreover, the accommodation coefficients appeared to be very similar for different materials;[30] e.g., for Ar^+ bombardment on copper surfaces, values of 0.9–1 were obtained in the energy range of 50–4000 eV.[30] In the present study, we have assumed a value equal to 0.5, but later in this article we will check the effect of varying this parameter.

It should be mentioned that in general, and especially at low pressures and high temperature gradients, $T_{g(\mathrm{wall})}\neq T_{\mathrm{wall}}$, which is called ''temperature jump phenomenon.'' This boundary condition is solved by iteration, i.e., the first time $T_{g(\mathrm{wall})}$ is assumed$=T_{\mathrm{wall}}$ Then, from the heat transfer equation, $(\nabla T_g)_{\mathrm{wall}}$ is calculated, yielding a new boundary equation. This procedure is repeated until T_g, calculated with the heat transfer equation, satisfies the boundary condition at the walls.

For this boundary condition, the temperature at the walls must be known. This shifts the problem from an unknown gas temperature to the need to know the wall temperature. The latter is also rather uncertain, and cannot be measured in the commercial analytical GDMS and GD–OES instruments. However, the anode cell walls can be, to a good approximation, assumed at room temperature. The cathode, on the other hand, is expected to warm up considerably due to the energy input by the bombardment of heavy particles. The exact value is not known, but it can vary from room temperature to 600–800 K (deduced from the fact that the cathode sample sometimes starts to melt), and it will probably be higher at GD–OES conditions than at GDMS conditions. We will, therefore, assume a value of 300 K for the GDMS conditions (because the VG9000 cell is most often cooled with liquid nitrogen, which will probably compensate the warming up by heavy particle bombardment) and a value of around 600 K at the GD–OES conditions (where the cathode is only cooled with water, and there is more warming up due to the higher electrical power). A value of about 600 K was indeed measured by preliminary experiments based on a pyrometer that measures the (continuum) radiation in the range 2–2.6 μm.[31] Moreover, these experiments have revealed that the cathode temperature slightly increases with increasing power (from about 500 K at 10 W to about 640 K around 120 W). Although these experiments are probably subject to some errors due to unknown contributions of infrared emission from the plasma itself,[31] the obtained values seem realistic. Therefore, and also due to the lack of more accurate input data, the observed behavior of the cathode temperature increasing slightly with power is adopted here. Due to the large uncertainties in the cathode temperature, the effect of this parameter on the calculations will also be investigated later in this article.

D. Model network

Figure 2 shows a flowchart of the model network. This flowchart does not differ drastically from the one explaining our previous modeling network;[32,33] the only difference is the addition of a heat transfer model. We will therefore not go into detail about the entire modeling network, which can be found in Refs. 32 and 33. We will only explain how the present heat transfer model is added to this model network.

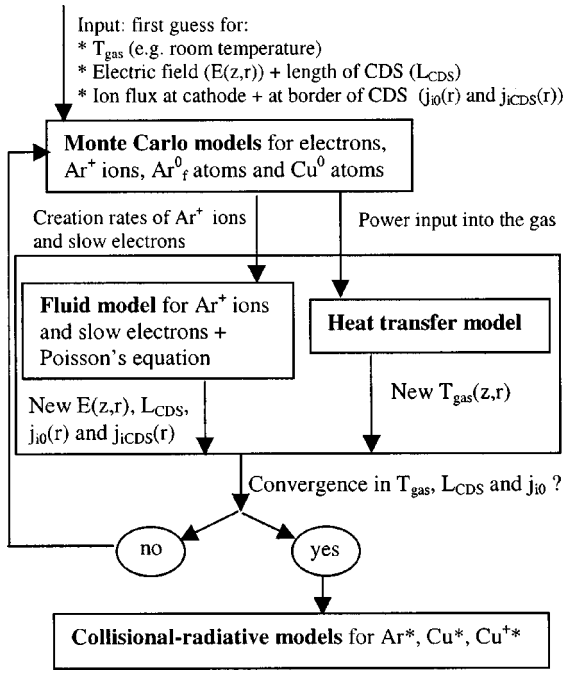

FIG. 2. Flowchart of the model network.

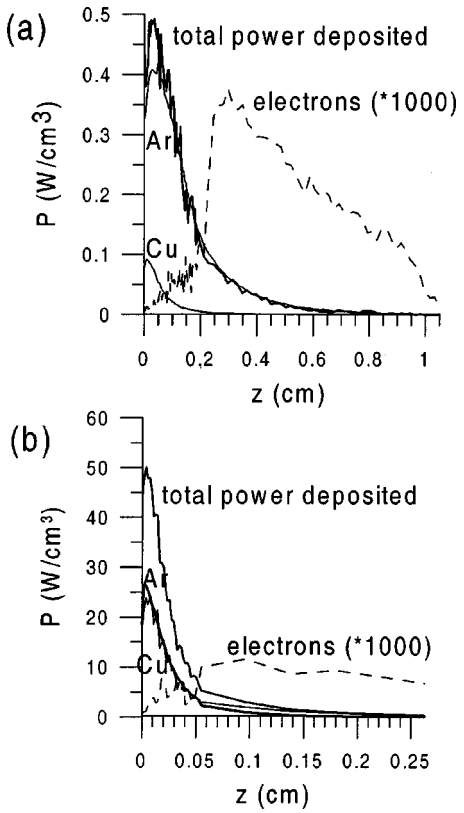

FIG. 3. Total power deposited in the argon gas as a function of axial distance from the cathode, as well as contributions of the Ar species, Cu atoms and electrons (enlarged by a factor of 1000), for the VG9000 cell (a) and the Grimm-type cell (b).

First, we assume a constant gas temperature, equal to the anode wall temperature. Moreover, a certain electric field distribution is assumed, as well as the thickness of the CDS, and the ion fluxes entering the CDS and bombarding the cathode. These values are needed to solve the Monte Carlo models (for Ar^+ ions, Ar^0_f atoms, and Cu^0 atoms and electrons). Output of these models are, on the one hand, the creation rates of Ar^+ ions and slow electrons, which are used in the fluid model (see e.g., Refs. 5, 9, and 33); and on the other hand, the power input, needed to calculate the temperature rise in the heat transfer model, as described earlier. Then, the new gas temperature (which defines the new gas density, based on $n=p/kT$, where the pressure p is assumed constant: hence, it determines the number of collisions in the Monte Carlo models), as well as the new electric field distribution, CDS length, and Ar ion fluxes entering the CDS and bombarding the cathode, are introduced again in the Monte Carlo models. The latter give new Ar^+ ion and electron creation rates and power input, which are again used in the fluid and heat transfer models, respectively. This procedure is repeated until convergence is reached, which happens after ~5 iterations. Finally, the earlier models can be further coupled to the collisional-radiative models describing the other plasma species (Ar excited atoms, Cu excited atoms, and Cu ions), because the latter do not have real influence on the earlier described models at the discharge conditions under study.

III. RESULTS AND DISCUSSION

A. Power input into the argon gas:

Figure 3(a) shows the power deposition into the argon gas, as a function of distance from the cathode, in the VG9000 cell for typical GDMS conditions: 1000 V, 4 mA and 75 Pa. It is clear that most of the power is deposited very close to the cathode, in the CDS (which is about 2 mm thick at the present conditions). The contribution of Ar species (ions and atoms) is clearly dominant (~87%), and is mainly due to kinetic energy transfer collisions and subsequent thermalization of the fast Ar atoms. The sputtered Cu atoms have a contribution of about 13%, but they play a significant role in only the first 2 mm from the cathode, because at further distances they are nearly all thermalized. The power input due to electron collisions (enlarged by a factor of 1000) takes place throughout the whole NG, but its contribution is actually negligible (~0.4%) compared to the heavy particles' collisions, due to their much lower mass and hence, inefficient energy transfer to the argon gas.

The power deposition in the Grimm-type cell as a function of axial distance from the cathode, is depicted in Fig. 3(b), for typical GD–OES conditions (800 V, 400 Pa, and 52 mA). Again, most of the power is deposited very close to the cathode (note the x axis: only the first 2.5 mm adjacent to the cathode are shown) and the decreasing power deposition with increasing distance is even more pronounced than for the GDMS conditions. Indeed, at the higher pressures, the sputtered Cu atoms lose their energies more efficiently in collisions, and become thermalized at distances closer to the cathode. Moreover, the CDS is considerably thinner at these higher pressures (order of 0.3–0.5 mm), so that the energy transfer from Ar^+ ions and Ar^0_f atoms also takes place closer to the cathode. Another difference with Fig. 3(a) is that the contributions of Ar species and Cu atoms become more com-

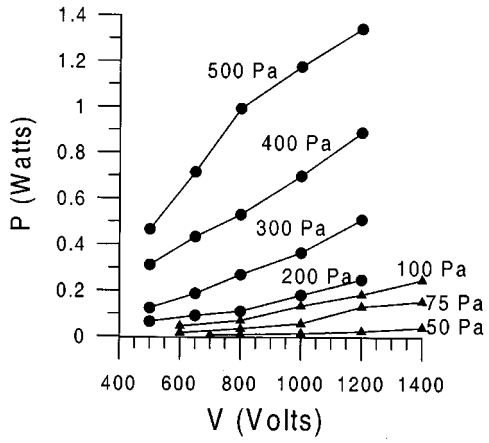

FIG. 4. Total deposited power integrated over the entire discharge cell, as a function of voltage, for a range of different pressures (the pressures common for the Grimm-type cell are represented by the full circles, whereas the typical pressures for the VG9000 cell are symbolized with the triangles).

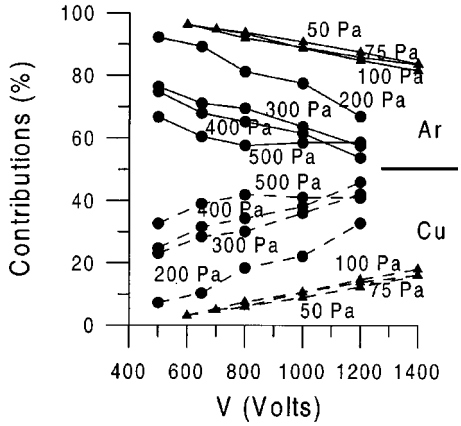

FIG. 5. Relative contributions of the Ar atoms (full lines) and Cu atoms (dashed lines) to the total power deposition, as a function of voltage for a range of different pressures. The pressures common for the Grimm-type cell are represented by the full circles, whereas the typical pressures for the VG9000 cell are symbolized with the triangles.

parable to each other, i.e., ~65% for the Ar species (which is again almost entirely due to elastic collisions and thermalization of Ar_f^0 atoms) and ~34.5% for the Cu species. The electrons contribute again about 0.4%, with a maximum in the beginning of the NG. The obtained power deposition behavior is in fairly good agreement with the calculation results of Ref. 24 although the discharge conditions are completely different (dc glow discharge with pressures in the millitorr regime). Indeed, in Ref. 24 most of the power was also deposited in the CDS, and the major contribution was also due to fast Ar atoms, followed by sputtered atoms; the contribution of Ar^+ ions was of much lower importance, and the possible gas heating due to electrons was not taken into account. Hence, it seems that both the region of maximum power deposition and the importance of different gas heating mechanisms are very similar, in spite of the totally different operating conditions.

In Fig. 4 the total power deposition (in watts) is plotted against discharge voltage, for a range of different pressures. The three lower pressures (indicated with the triangles) are typical for GDMS, whereas the four higher pressures (symbolized with the full circles) are common for GD–OES. It is clear that the deposited power increases with rising voltage and pressure. This is quite logical because the current and the input power (current times voltage) become higher as well, and more power input in the discharge enables more power deposited into the argon gas. The total deposited power varies from 0.005 W at the lowest pressure and voltage investigated to 1.3 W at the highest pressure and voltage under consideration. For all conditions investigated, the deposited power into the argon gas was about 1%–2% of the total input discharge power. This is considerably less than for the discharge conditions investigated in Ref. 24, where the power consumed for the gas heating was found to comprise more than 30% of the discharge input power.

Figure 5 illustrates the relative contributions of the Ar atoms and Cu atoms to the total power deposition. For all conditions under study the fast Ar atoms (solid lines) play a dominant role in the power deposition, but it should be noted that these fast Ar atoms are created by collisions of the Ar ions (and later on, of course also by collisions of the fast Ar atoms) and by collisions of the Cu atoms. Direct gas heating due to collisions of the Ar ions is negligible (less than 1%), but direct gas heating due to collisions of the sputtered Cu atoms (dashed lines in the figure) is quite important, and its contribution clearly increases with rising pressure and voltage. At the highest pressures and voltages investigated, the contribution of the Cu atoms becomes almost comparable to the contribution of the Ar atoms. The gas heating due to electrons plays only a minor role (about 0.2%–0.6%) at the conditions under study.

B. Resulting gas temperature:

Figure 6 shows the resulting gas temperature corresponding to the power deposition depicted in Fig. 3, for both the VG9000 cell (a) and the Grimm cell (b), at the same discharge conditions as in Fig. 3. The cathode (sample) is found at the left end of both figures. The black rectangles in Fig. 6(a) symbolize the insulating ring (at $z=0-0.05$ cm) and the anode front plate (between $z=0.05$ and $z=0.15$ cm), whereas the other cell borders are at anode potential [see Fig. 1(a)]. In the case of the Grimm-type cell, only the first 1.5 cm from the cathode is shown, since the calculations predict a temperature rise above room temperature only in this region. Indeed, the plasma is most intense in the first centimeter from the cathode, and therefore nearly all collisions (and gas heating mechanisms) take place in this region. As mentioned before, we assumed that the anode walls are all at room temperature. The same is also assumed for the cathode in the VG9000 cell. However, for the Grimm cell at the present conditions, we assumed a cathode temperature of 570 K, due to less efficient cooling and more energy input due to heavy particle bombardment.

As is seen in Fig. 6(a), the gas temperature rises above room temperature by about 30 K, and reaches a maximum of about 330 K at 1–2 mm from the cathode; then it decreases slightly to room temperature at the cell walls. The tempera-

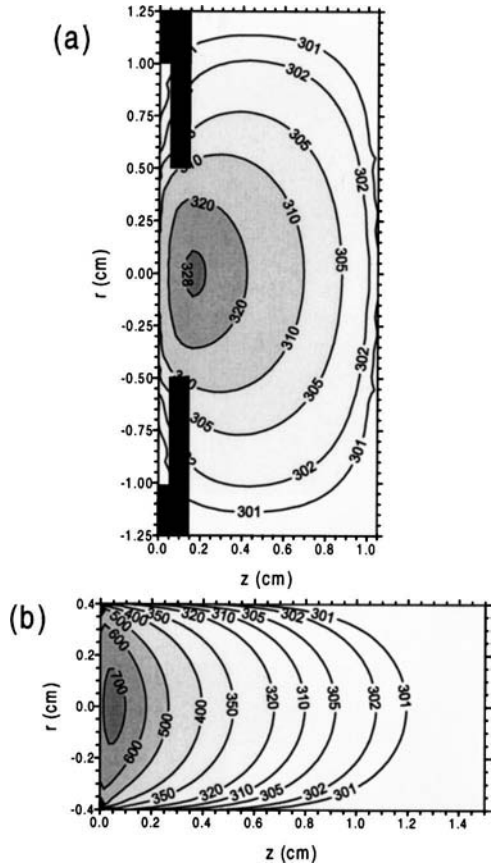

FIG. 6. Resulting two-dimensional gas temperature profile for the power deposition presented in Fig. 3, in the VG9000 cell (a) and the Grimm-type cell (b). The cathode is found at the left end of both figures, whereas the other borders of the figure represent the anode cell walls (grounded). The black rectangles in Fig. 6(a) symbolize the insulating ring (from $z=0$ to $z=0.05$ cm) and anode front plate (from $z=0.05$ to $z=0.15$ cm). In Fig. 6(b), not the entire cell geometry but only the first 1.5 cm from the cathode is shown, because the gas heating was found to be negligible at larger distances from the cathode.

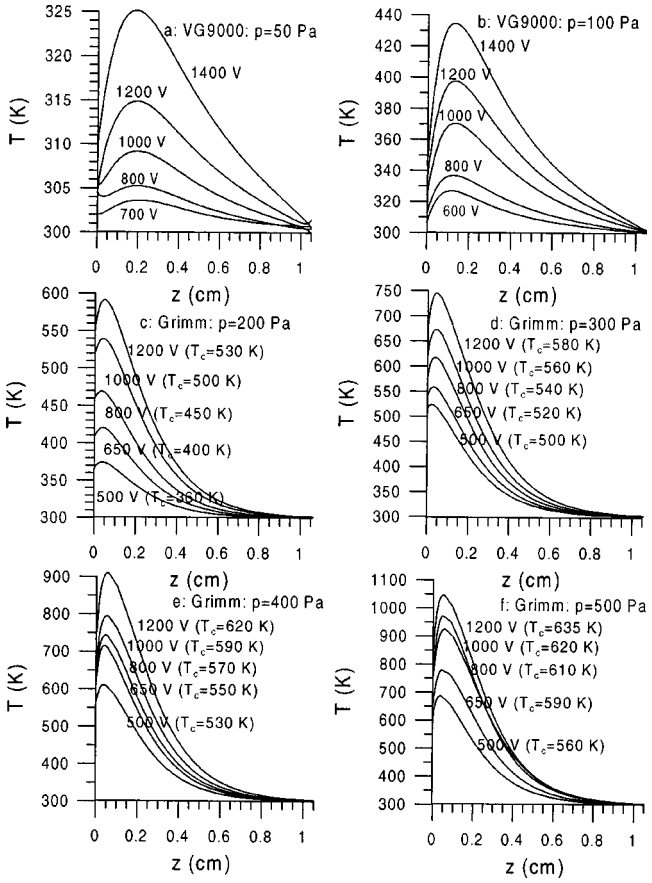

FIG. 7. One-dimensional gas temperature profiles for a range of different voltages and pressures. Figures (a) and (b) have been calculated in the VG9000 cell, whereas Figs. (c)–(f) apply to the Grimm-type cell. The temperature value assumed at the anode walls is 300 K; the cathode temperature is 300 K in the VG9000 cell, and the temperature values used for the cathode in the Grimm-cell are indicated for each curve in Figs. (c)–(f).

ture rise is much more significant in the case of the GD–OES conditions [see Fig. 6(b)]. Indeed, the temperature reaches a maximum of almost 750 K, which is 180 K above the cathode temperature, and 450 K above the anode temperature. The maximum is located closer to the cathode (at ~0.5 mm) because the power deposition was also concentrated very close to the cathode [see Fig. 3(b)]. The gas temperature decreases also gradually to room temperature at about 1–1.5 cm from the cathode.

The one-dimensional gas temperature profiles as a function of axial distance from the cathode are presented in Fig. 7 for a range of different voltages and pressures. The pressure values of 50 and 100 Pa are typical for GDMS whereas the other pressures are more common for GD–OES. The profiles look qualitatively similar for all conditions investigated, with a maximum in the first millimeter from the cathode and a decrease to room temperature at about 1 cm from the cathode. Hence, a distinct difference with the low-pressure glow discharge is found. Indeed, although the power deposition took place in the CDS for both our conditions and the conditions in Ref. 24, the maximum gas temperature in the latter case was found in the middle of the discharge cell, although the profile was still asymmetric towards the cathode. The reason for this difference is probably the lower pressure, which facilitates the transport of energy to the middle of the discharge. The gas temperature rises with pressure and with voltage, due to an increased power deposition (see Fig. 4).

It is also significant that the gas temperature adjacent to the cathode is clearly higher than the cathode temperature. For the VG9000 cell (pressures of 50 and 100 Pa), the cathode temperature was assumed 300 K, whereas the gas temperature adjacent to the cathode ranged from 302 K at the lowest pressure and voltage to 345 K at the highest pressure and voltage investigated, which means a ''temperature jump'' of 2–45 K. For the Grimm cell, the cathode temperature was assumed to range from 360 K (at 200 Pa and 500 V) until 635 K (at 500 P and 1200 V), increasing with discharge power according to Ref. 31. The exact values used in the calculations, based on the data in Ref. 31, are indicated in Fig. 7. The gas temperature adjacent to the cathode was, however, also clearly higher than the cathode temperature (see Fig. 7), with a temperature jump varying from 7 K at low pressure and voltage to 200 K at the highest pressure and voltage investigated.

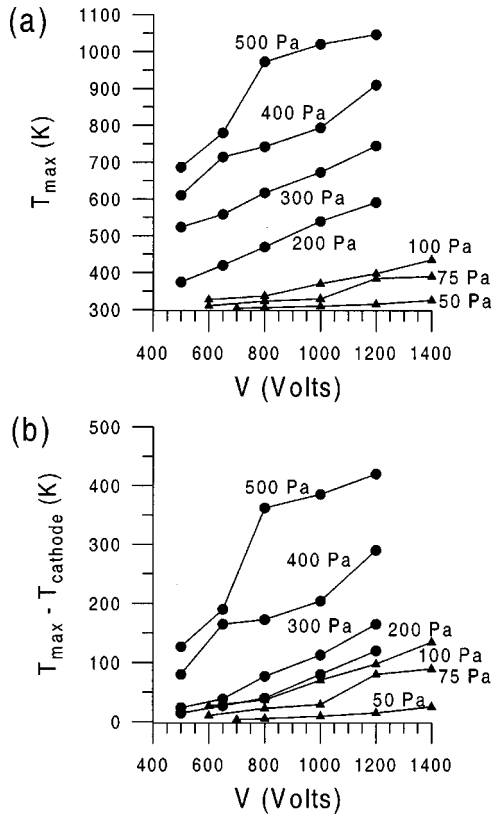

FIG. 8. Gas temperatures at the maximum of their profiles (a) and temperature increase of this maximum compared to the cathode temperature (b), as a function of voltage for a range of different pressures. The pressures common for the Grimm-type cell are represented by the full circles, whereas the typical pressures for the VG9000 cell are symbolized with the triangles.

The gas temperature at the maximum of its profile varied from only 303 K at 700 V and 50 Pa until roughly 1050 K at 1200 V and 500 Pa, which means an increase compared to the cathode temperature ranging from only 3 to about 400 K, rising with pressure and voltage. The relative temperature increase, compared to the cathode temperature, varies, hence, from about 1% at the lowest voltage and pressure under study (i.e., 303 K gas temperature compared to 300 K cathode temperature) to ~65% at the highest voltage and pressure investigated (i.e., about 1050 K gas temperature compared to 635 K cathode temperature). For the glow discharge, magnetron and inductively coupled plasma conditions in the millitorr range, where gas heating has been studied in most detail, temperature rises are reported ranging from 3%–50%[16,17,22,24] to a factor of 2[16,21] and 3.[19,23]

The calculated temperatures for the VG9000 cell are in fairly good agreement with the one-dimensional calculation results of Ref. 25, both the temperature profile (i.e., a maximum in the CDS), and the absolute values. Our results for the Grimm-type cell appear to be somewhat lower than the experimental data of Ref. 15, but the temperature profiles (with a maximum adjacent to the cathode) and the trend as a function of discharge conditions are in reasonable agreement.

The gas temperature at the maximum of its profile is also illustrated in Fig. 8(a), for a range of different pressures. The gas temperature increases more or less linearly with voltage. It should, however, be mentioned that the exact values of these gas temperatures are subject to some uncertainties, due to the value of the cathode temperature that is actually unknown. The net temperature rise compared to the cathode temperature is probably a more reliable calculated quantity. Indeed, although we found that a higher assumed value of the cathode temperature yielded a somewhat lower temperature rise for the same amount of power deposition and the same anode temperature, the difference was only about 20 K for a variation of the cathode temperature over 100 K and more (see later; Fig. 10). Therefore, Fig. 8(b) depicts the temperature rise compared to the cathode temperature as a function of voltage and pressure. The temperature rise increases with voltage and pressure. The difference between 100 and 200 Pa seems to be very small, but this is due to a higher assumed cathode temperature in the Grimm cell than in the VG9000 cell, which artificially allows less net temperature rise, although the absolute gas temperature is still higher. It appears from Fig. 8(b) that the net temperature rise varies from a few to 400 K.

C. Effect of the temperature rise on the electrical characteristics:

When the gas pressure and temperature and the voltage are given as inputs in our model, the electrical current is calculated self-consistently as the sum of the fluxes of the charged plasma species (i.e., mainly electrons and argon ions). We found previously that both gas pressure and temperature have a rather strong effect on the calculated current. Indeed, the gas temperature and pressure determine the argon gas density, through $n=p/kT$. The latter directly influences the number of ionization collisions, and hence, creation of new electrons and argon ions, and from this, the calculated electrical current. It is expected that the gas temperature rise which we have calculated here and which yields a lower gas density, will result in a lower electrical current. For example, for the VG9000 cell we found that a constant gas temperature of 300 K yielded, for the same conditions of voltage and pressure as in Figs. 3(a) and 6(a) (1000 V, 75 Pa) a calculated electrical current of 5.5 mA. The gas temperature profile calculated for these conditions and presented in Fig. 6(a), resulted in a current of 4 mA, hence 27% lower. However, besides the drop in the absolute values of the current, the slope of the current–voltage characteristics remained very similar to the calculations we performed before, assuming a constant gas temperature (see e.g., Ref. 13). Indeed, the presently calculated gas temperatures did increase only moderately with pressure and voltage for the VG9000 conditions. Hence, their effect on the calculated currents was comparable for all pressures and voltages investigated.

A different behavior is observed for the Grimm-cell conditions. Indeed, the temperature rises here to considerable values, and this has a significant effect on the calculated current–voltage characteristics. Figure 9 presents the calculated currents as a function of voltage, for different pressures. The solid black lines with full black circles illustrate the calculated results in the present work, whereas the dashed gray lines with gray squares represent current–voltage characteristics that we have calculated previously, with the gas

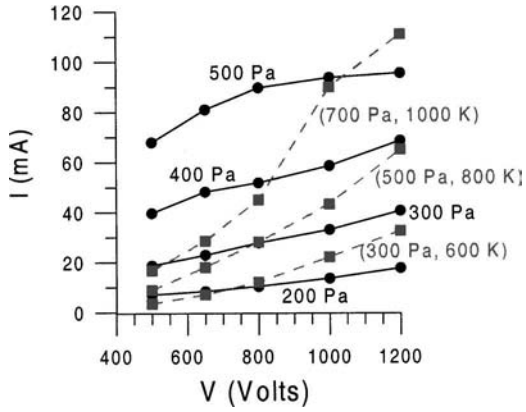

FIG. 9. Calculated current–voltage characteristics for different pressures in the Grimm-type cell. The black solid lines with black full circles illustrate the present calculation results, whereas the gray dashed lines with gray squares represent previous calculations with constant gas temperature (indicated between brackets).

pressure and temperature (assumed constant) indicated between brackets (results adopted from Ref. 34). The old data predicted a more than linear (almost quadratic) increase of the current with rising voltage. However, experimentally the power is found to rise linearly with voltage,[35] which means a less than linear increase of current as a function of voltage and even saturation of the current at high voltages. The present calculation results are, therefore, a better prediction of the experimentally observed behavior. Indeed, since the gas temperature increases significantly with rising voltage and pressure, the gas density drops correspondingly, giving rise to less ionization collisions, and hence, a lower current than would be expected at constant gas temperature. The reason for the higher absolute values of the calculated current at 500 Pa now compared to the old values is due to the assumption that the gas temperature at this pressure was 800 K (constant in the entire discharge plasma). This is, except at the maximum of the temperature profile, generally higher than the gas temperature we calculated in the present work. Hence, the absolute values should be considered with caution, due to the uncertainties in the gas temperature and the cathode temperature. However, it is clear from Fig. 9 that the presently calculated gas temperature profiles strongly affect the calculated current–voltage characteristics, which illustrates the importance to obtain a better knowledge of this quantity.

Finally, when the gas temperature affects the absolute value of the electrical current, also other plasma quantities, like the species densities, will change slightly. However, the relative profiles of most plasma quantities remain unaffected.

D. Parametric study: Effect of the thermal accommodation coefficient α, the cathode temperature, and the threshold energy between the Ar_f^0 beam and the bulk Ar gas

Because the exact values of the thermal accommodation coefficient and the cathode temperature are not known, it is important to investigate their effect on the resulting gas temperature. Moreover, we have studied the effect of the choice

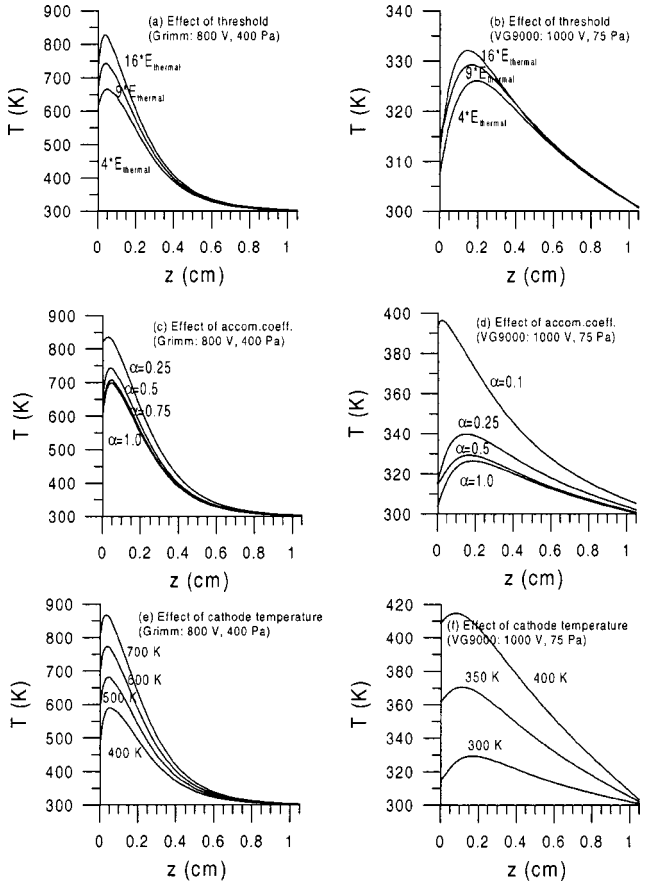

FIG. 10. One-dimensional gas temperature profiles for different input values of the threshold energy [Figs. (a) and (b)], the thermal accommodation coefficient [Figs. (c) and (d)] and the cathode temperature [Figs. (e) and (f)]. Figures (a), (c) and (e) have been calculated in the Grimm-type cell, whereas Figs. (b), (d), and (f) apply to the VG9000 cell.

of the threshold energy between the Ar_f^0 beam and the bulk Ar gas. Figure 10 illustrates the effect of these input parameters for both the Grimm and the VG9000 cell.

Figures 10(a) and 10(b) demonstrate that choosing a higher threshold energy for subdivision between gas heating and formation of fast Ar atoms yields a higher gas temperature. Indeed, more energy will be transferred to the argon gas, resulting in a higher gas temperature. The effect is rather high for the Grimm-cell conditions: The maximum temperature increases from about 670 K (for $E_{\text{threshold}}$ equal to $4E_{\text{thermal}}$), to 743 K (for $E_{\text{threshold}}$ equal to $9E_{\text{thermal}}$), and to 827 K (for $E_{\text{threshold}}$ equal to $16E_{\text{thermal}}$), hence a difference of 160 K between the highest and lowest value. Compared to the absolute values, the difference is, however, only about 20%. For the VG9000 conditions, the effect is of minor importance: The maximum temperature varies between 326 and 332 K (hence, only a few percent in relative terms) for the same variations in threshold values as in the Grimm case. We used a threshold energy equal to nine times the thermal energy throughout all our calculations, and it should be borne in mind that changing this assumption has some effect on the calculation results.

The effect of the thermal accommodation coefficient α is shown in Figs. 10(c) and 10(d), for the Grimm and the VG9000 cell. Varying α between 1 and 0.5 does not affect

the calculated results to a large extent, neither for the Grimm cell nor for the VG9000 cell. However, changing α to lower values has more effect on the resulting temperature profiles. The difference between $\alpha=0.5$ and 0.25 is clearly higher than between $\alpha=0.5$ and 1; at $\alpha=0.1$ the calculated temperature is significantly higher, and moreover the temperature profile exhibits a maximum at the cathode, in the VG9000 cell. In the Grimm cell, the temperature calculations for $\alpha=0.1$ yielded unrealistically high results, probably due to numerical instability problems. We used a value for α of 0.5, but it is clear that a higher value would yield more or less the same calculation results. This observation is reassuring, because the values found in the literature varied generally between 0.5 and 1; only below 10 eV, lower values were obtained.[29]

Finally, the temperature profiles for different assumptions of the cathode temperature are plotted in Figs. 10(e) and 10(f). It appears that increasing the cathode temperature to a certain degree yields a similar but slightly lower increase in the maximum gas temperature (e.g., 80–95 K increase in gas temperature for a cathode temperature rise of 100 K). Hence, the net increase in gas temperature depends only slightly on the cathode temperature, but the final value of the gas temperature is definitely determined by the cathode temperature. Since the latter values are actually unknown, forcing us to use educated guesses, the absolute values of the gas temperature can be subject to considerable errors, i.e., the error in the calculated gas temperature is as large as the error in the input cathode temperature. As long as this value is not accurately known, the actual value of the gas temperature has to be considered with caution. Nevertheless, the calculated temperature rise compared to the cathode temperature, and the increasing trend with pressure and voltage, are fairly reliable. Moreover, the calculated current–voltage characteristics show reasonable values, which suggests that the calculated gas temperatures are quite realistic.

IV. CONCLUSION

We have developed a model to calculate the gas temperature in a direct current glow discharge in argon with copper cathode, which is commonly used in analytical spectroscopy. Typical operating conditions investigated here are 50–500 Pa, 500–1400 V, and 1–100 mA. The energy transfer (or deposited power) to the argon gas due to elastic collisions of the Ar^+ ions, Ar_f^0 fast atoms, and sputtered Cu atoms and electrons is calculated in Monte Carlo models. This energy transfer rate is then used in a heat transfer model to calculate the resulting gas temperature.

The total power deposited into the argon gas ranges from 0.005 to 1.3 W, increasing considerably with voltage and pressure, but at all conditions investigated, it amounts to about 1%–2% of the total input power in the discharge. This power deposition mainly takes place in the first millimeter from the cathode. The majority of the deposited power originates from energy transfer collisions and subsequent thermalization of the fast Ar_f^0 atoms, which have been formed by collisions of the Ar^+ ions and the Cu atoms. However, direct energy input into the gas due to elastic collisions of the Cu atoms is also an important source for the gas heating, and its contribution becomes almost comparable to the contribution of fast Ar atoms at high pressure and voltage.

The calculated gas temperature as a result of this power input shows a maximum at 0.5–2 mm from the cathode, and decreases gradually to room temperature at about 1 cm from the cathode and at the anode walls. This gas temperature is only slightly above room temperature at the lowest pressure and voltage investigated (50 Pa, 700 V), but it increases clearly with rising voltage and pressures, and takes values of about 1000 K at its maximum for the highest pressure and voltage under consideration (500 Pa, 1200 V). Also the temperature rise with respect to the cathode temperature was calculated, and it was found to vary between a few kelvin at low voltage and pressure to about 400 K at the highest pressure and voltage under study.

Since the gas temperature, together with the pressure, determine the calculated electrical current through the gas density and the number of ionization collisions, we have also calculated current–voltage characteristics at a range of pressures. At the low pressures typical for the VG9000 cell, the change in the gas temperature is only moderate and its effect on the current–voltage characteristics is not important. However, at the high pressures commonly used in the Grimm-type source, the gas temperatures rise considerably. As a result, the current does not increase rapidly with voltage, which is in better qualitative agreement with experimental observations than in the case when the temperature is assumed constant.

Finally, because the exact values of the input parameters, like the threshold energy for gas heating, the thermal accommodation coefficient, and the cathode temperature are unknown, we have simulated their effect on the calculated results, in order to obtain a feeling of the expected uncertainties in the results. The cathode temperature is especially important in determining the final calculated gas temperature; indeed, the latter increases to almost the same extent as the cathode temperature. Hence, errors in the input cathode temperature, of which the actual value is unknown, are also reflected in the calculated gas temperatures. Therefore, the absolute values of our calculated gas temperatures should be considered with caution, but the net temperature rise with respect to the cathode temperature, as well as the trends as a function of voltage and pressure, are expected to be reliable.

ACKNOWLEDGMENTS

A. Bogaerts is indebted to the Flemish Fund for Scientific Research (FWO) for financial support. The authors also acknowledge financial support from the Federal Services for Scientific, Cultural and Technical Affairs of the Prime Minister's Office through IUAP (Conv. P4/10). Finally, we also thank D. Hodoroaba for supplying us with his preliminary results on cathode temperature measurements, and C. Abrams for reading the article and giving useful suggestions for improvement of the English.

[1] R. K. Marcus, *Glow Discharge Spectroscopies* (Plenum, New York, 1993).
[2] R. Payling, D. G. Jones, and A. Bengtson, *Glow Discharge Optical Emission Spectrometry* (Wiley, Chichester, 1997).
[3] A. Bogaerts, M. van Straaten, and R. Gijbels, Spectrochim. Acta B **50**, 179 (1995).
[4] A. Bogaerts, M. van Straaten, and R. Gijbels, J. Appl. Phys. **77**, 1868 (1995).
[5] A. Bogaerts, R. Gijbels, and W. J. Goedheer, J. Appl. Phys. **78**, 2233 (1995).
[6] A. Bogaerts and R. Gijbels, Phys. Rev. A **52**, 3743 (1995).
[7] A. Bogaerts and R. Gijbels, J. Appl. Phys. **78**, 6427 (1995).
[8] A. Bogaerts and R. Gijbels, J. Appl. Phys. **79**, 1279 (1996).
[9] A. Bogaerts, R. Gijbels, and W. J. Goedheer, Anal. Chem. **68**, 2296 (1996).
[10] A. Bogaerts and R. Gijbels, Anal. Chem. **68**, 2676 (1996).
[11] A. Bogaerts, R. Gijbels, and J. Vlcek, J. Appl. Phys. **84**, 121 (1998).
[12] A. Bogaerts, R. Gijbels, and R. J. Carman, Spectrochim. Acta B **53**, 1697 (1998).
[13] A. Bogaerts, Plasma Sources Sci. Technol. **8**, 210 (1999).
[14] A. Bogaerts and R. Gijbels, J. Appl. Phys. **86**, 4124 (1999).
[15] N. P. Ferreira, H. G. C. Human, and L. R. P. Butler, Spectrochim. Acta B **35**, 287 (1980).
[16] S. M. Rossnagel, J. Vac. Sci. Technol. A **6**, 19 (1988).
[17] T. Hori, M. D. Bowden, K. Uchino, K. Muraoka, and M. Maeda, J. Vac. Sci. Technol. A **14**, 144 (1996).
[18] K. Muroaka, K. Uchino, and M. D. Bowden, Plasma Phys. Controlled Fusion **40**, 1221 (1998).
[19] J. D. Bukowski, D. B. Graves, and P. Vitello, J. Appl. Phys. **80**, 2614 (1996).
[20] G. M. Petrov and C. M. Ferreira, Phys. Rev. E **59**, 3571 (1999).
[21] H. M. Urbassek and D. Sibold, J. Vac. Sci. Technol. A **11**, 676 (1993).
[22] A. Kersch, W. Morokoff, and S. Werner, J. Appl. Phys. **75**, 2278 (1994).
[23] G. M. Turner, J. Vac. Sci. Technol. A **13**, 2161 (1995).
[24] V. V. Serikov and K. Nanbu, J. Appl. Phys. **82**, 5948 (1997).
[25] I. Revel, L. C. Pitchford, and J. P. Boeuf, Poster at the XXIV International Conference on Phenomena in Ionized Gases, Warsaw, Poland, 1999, Proceedings of Contributed Papers, vol. III, p. 39.
[26] V. V. Serikov, S. Kawamoto, and K. Nanbu, IEEE Trans. Plasma Sci. **27**, 1389 (1999).
[27] A. V. Phelps, J. Appl. Phys. **76**, 747 (1994).
[28] S. S. Sazhin and V. V. Serikov, Planet. Space Sci. **45**, 361 (1997).
[29] H. F. Winters, H. Coufal, C. T. Rettner, and D. S. Bethune, Phys. Rev. B **41**, 6240 (1990).
[30] H. Coufal, H. F. Winters, E. Bay, and W. Eckstein, Phys. Rev. B **44**, 4747 (1991).
[31] D. Hodoroaba (private communication).
[32] A. Bogaerts, Ph.D. Dissertation, University of Antwerp, 1996.
[33] A. Bogaerts and R. Gijbels, Plasma Phys. Rep. **24**, 573 (1998).
[34] A. Bogaerts and R. Gijbels, Spectrochim. Acta B **53**, 437 (1998).
[35] V. Hoffmann, F. Prässler, K. Wetzig, D. Schiel, and R. Jährling, Poster at the 1998 Winter Conference on Plasma Spectrochemistry, Scottsdale, Arizona, 1998.